IEEE Access
Multidisciplinary | Rapid Review | Open Access Journal

Received May 9, 2018, accepted June 10, 2018, date of publication June 15, 2018, date of current version July 12, 2018.

Digital Object Identifier 10.1109/ACCESS.2018.2847637

Intelligent Electro-Pneumatic Position Tracking System Using Improved Mode-Switching Sliding Control With Fuzzy Nonlinear Gain

ZHONGLIN LIN, TIANHONG ZHANG, QI XIE, AND QINGYAN WEI

Jiangsu Province Key Laboratory of Aerospace Power System, College of Energy and Power Engineering, Nanjing University of Aeronautics and Astronautics, Nanjing, Jiangsu 210016, China

Corresponding author: Tianhong Zhang (thz@nuaa.edu.cn)

This work was supported in part by the Funding of Jiangsu Innovation Program for Graduate Education and the Fundamental Research Funds for the Central Universities under Grant KYLX16_0396, in part by the Fundamental Research Funds for the Central Universities under Grant NS2018012, in part by the Aeronautical Science Foundation of China under Grant 2016ZD52038, and in part by the National Nature Science Foundation of China under Grant 51576097.

ABSTRACT In this paper, a mode-switching sliding controller with the nonlinear gain generated by a fuzzy logic controller is put forward to enhance the tracking performance in an electro-pneumatic position control system which includes four solenoid ON–OFF valves and a double rod-end cylinder. The proposed method is designed to increase the response speed and reduce the overshoots by utilizing the nonlinear gain which is determined by a fuzzy logic controller. In addition, several improvements are made in the mode-switching sliding controller originally from previous works. The mode-switching strategy is totally redesigned and a hysteresis control scheme is introduced to the new mode-switching sliding controller. Moreover, the improved controller is properly combined with the fuzzy nonlinear gain. Simulation and experiments with various kinds of input are carried out to verify the effectiveness of the proposed method. All the experiments are conducted on a field programmable gate array platform, and the experimental results validate the reliability of the novel scheme.

INDEX TERMS Electro-pneumatic position control, fuzzy logic control, nonlinear gain, ON–OFF valve, sliding mode control.

I. INTRODUCTION

Pneumatic systems which use compressed air as the source of power have been accepted by almost all branches of industry such as aviation, drilling platform, missile guidance, and robotics over the past ten years. Compared to the hydraulic system, the pneumatic system has the advantages of clean environment, no fire hazard, and easy maintenance. The pneumatic control valve, which is regarded as the interface between fluid flow and electronic controls, is widely studied in recent researches. In traditional servo-pneumatic systems, proportional valve is utilized as the primary control component for its proportional input-output characteristic [1]–[3]. Whereas, the associated disadvantages including bulkiness, complex structures, and high cost make it difficult to be used widely. Therefore, the relatively portable, simple structured and cheap solenoid on-off valve is applied in more and more servo-pneumatic control systems [4]–[6].

The Pulse Width Modulation (PWM) method is used to apply the solenoid on-off valves in the servo-pneumatic control systems instead of the proportional valves [7], [8]. The PWM inputs for the on-off valves make the valves open and close completely and continuously. The PWM-driven on-off valves can get the similar proportional behavior of the servo valves [9], [10]. However, the dead-zone problem still restricts the advancement of the method [11]–[13]. Meanwhile, another conventional method to drive the on-off valves is the mode-switching method. Nguyen *et al.* [14] initially use the three-mode method without PWM method in a pneumatic motion control system using four on-off valves and a rodless cylinder. The control method performs well, and low steady-state errors are observed. On the basis of T. Nguyen *et al.*, five-mode and seven-mode methods are proposed by Hodgson *et al.* [15]. In the experimental results of Hodgson *et al.*, about 18% positive overshoot is observed in the three-mode method and 1.9% positive overshoot in the seven-mode method. About 5% negative overshoot is found in the seven-mode method. Based on these researches, an improved mode-switching strategy is introduced in this

article. In the new mode-switching strategy, the simple seven-mode strategy is combined with the hysteresis controller and the PWM-driven method.

Many advanced control approaches such as proportional-integral-derivative (PID) control, fuzzy logic control (FLC), sliding mode control (SMC), and model predictive control (MPC) have been researched in the pneumatic control systems since the 1990s [16]–[21]. Conventional PID controller, which is regarded as a linear controller, is not suitable for the highly nonlinear pneumatic system. The nonlinear PID (NPID) and multi-rate NPID (MN-PID) controller are put forward to deal with the high nonlinearities caused by the system dynamics and the strong compressibility of the gas [22], [23]. The concept of automatic nonlinear gain is proposed in these articles to enhance the original control method and add flexibility to the controller. The way of obtaining the nonlinear gain automatically is using a fuzzy logic controller which is widely used in pneumatic control systems [17], [24]. These approaches are especially valid in tracking experiments with variable payloads. Payloads of up to 20 kg are successfully handled by the NPID controller, and the conventional PID controller fails to deal with payloads of more than 5 kg [22]. The MN-PID controller can handle payloads of 24 kg at most, and the absolute errors are relatively low [23]. Whereas, these approaches are only studied in the pneumatic systems using proportional valves, and the performance of the systems using on-off valves is still unknown. For on-off valves, sliding mode controller is quite effective. The most significant advantage of sliding mode control is the robustness to the uncertainty of the pneumatic models [15], [25]. This paper is targeted on designing the new mode-switching strategy on a sliding mode controller. The sliding controller is properly combined with the fuzzy nonlinear gain which is generated by a fuzzy logic controller. Additionally, field programmable gate array (FPGA) platforms are barely applied in conventional electro-pneumatic systems, and only three papers are found using FPGA in the field of electro-pneumatic tracking systems [3], [26], [27]. FPGA platform is used in the article as the primary control platform for real-time control.

In this research, a mode-switching sliding controller with the nonlinear gain generated by a fuzzy logic controller is presented to improve the tracking performance by reducing overshoots and increasing response speed in tracking different kinds of reference. Indeed, the nonlinear gain is an enhancement for the sliding controller, and it is proved to be valid with various payloads in the experiments. The studied pneumatic tracking system consists of four fast solenoid valves and a double rod-end cylinder. The following article is organized as: in Section II, mathematical models of the on-off valve, chambers, and piston are introduced. The integrated model is also introduced at the end of the section. In Section III, controller designs for the position tracking system including fuzzy nonlinear gain, mode-switching strategy, sliding mode controller, and parameters selection are introduced. Simulation results are shown after the controller designs. Section IV introduces the experimental setup. The experimental results are expressed in Section V as well as the related discussions. At last, Section VI presents the conclusion of the research.

II. MATHEMATICAL MODELING

The real-time position tracking system employed in this article consists of four 2-2 solenoid on-off valves, a double rod-end cylinder, and a sliding table, as shown in Fig. 1. Two valves are configured as the inlet valves and the others are configured as the outlet valves. The payloads are installed on the sliding table which is attached to the push rod of the cylinder. Several assumptions are made for the modeling: air in the system is ideal gas; gas density in the chambers and pipes is uniform; the air flow process is adiabatic; all the gas leaks are negligible; the temperature change inside the chambers is negligible with respect to the temperature of the air supply; the pressures of the air supply and the atmosphere are constant; the stiction force of the piston is negligible since the experimental actuator is anti-stiction. The models of the on-off valve and the cylinder are introduced firstly. Then the integrated simulation frame is presented at the end of the section.

A. MODELING OF THE ON-OFF VALVE

The model of the solenoid on-off valve is traditionally divided into three parts: electromagnetism, mechanism, and fluid [28], [29]. The electromagnetic part drives the air pass over the valve orifice by the motion of the spool. The basic orifice equations of the valve are given by [30], [31]:

$$\begin{aligned}&\frac{\mathrm{d}m(P_{in}, P_{out})}{\mathrm{d}t}\\&= \dot{m}(P_{in}, P_{out})\\&= \begin{cases}\dfrac{0.0405 C_d P_{in} S}{\sqrt{T}}, & P_c \le P_{cr}\\ \dfrac{C_d P_{in} S}{\sqrt{T}} \sqrt{\dfrac{2\gamma}{R(\gamma-1)}\left((P_c)^{\frac{2}{\gamma}} - (P_c)^{\frac{\gamma+1}{\gamma}}\right)}, & P_c > P_{cr}\end{cases}\end{aligned} \tag{1}$$

where P_{in} is the input pressure of the valve, P_{out} is the output pressure of the valve, C_d is the discharge coefficient of the valve, S is the effective cross-sectional area of the orifice, T is the stagnation temperature, γ is the specific heat ratio, R is the ideal gas constant, $P_c = P_{out}/P_{in}$ is the specific pressure ratio, and P_{cr} is the critical pressure ratio. γ is 1.2 and P_{cr} is 0.528 according to Richer and Hurmuzlu [32] and Taghizadeh *et al.* [29], respectively. Equation (1) consists of two nonlinear equations for different regimes. As the strong compressibility of the air, when the specific ratio P_c is greater than the critical pressure ratio P_{cr}, the dynamics of the mass flow relies on the input and output pressure of the valve nonlinearly, and the regime is subsonic. Whereas, when P_c is smaller than P_{cr}, the dynamics become linear and rely on the input pressure. The air flow is in the sonic velocity (choked regime) in this condition. In both conditions, the mass flow relies linearly on the effective cross-sectional area of the orifice.

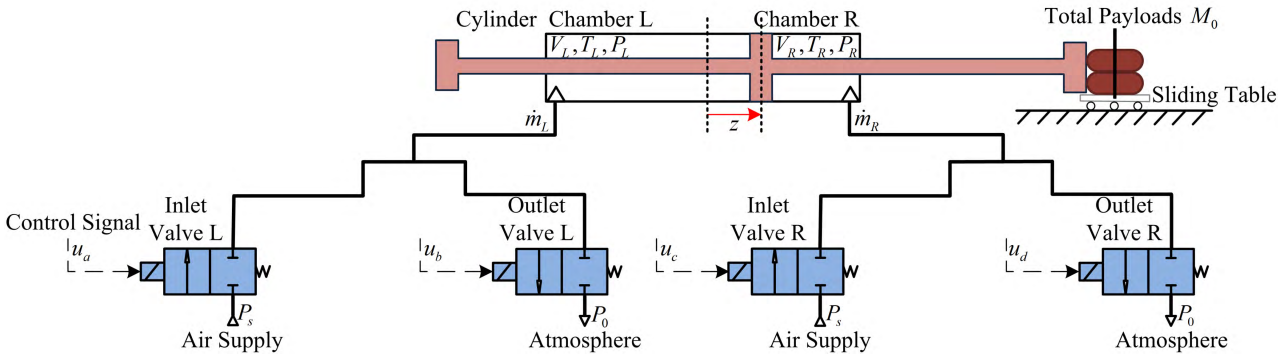

FIGURE 1. Schematic diagram of the system.

The mass flow rate $\dot{m}_L$ and $\dot{m}_R$ is described in terms of four control signals u_a, u_b, u_c, and u_d ($u_i \in \{0, 1\}$ and $i \in \{a, b, c, d\}$). The equations for $\dot{m}_L$ and $\dot{m}_R$ are given by:

$$\begin{cases} \dot{m}_L = u_a \dot{m}(P_s, P_L) - u_b \dot{m}(P_L, P_0) \\ \dot{m}_R = u_c \dot{m}(P_s, P_R) - u_d \dot{m}(P_R, P_0) \end{cases} \tag{2}$$

where P_s, P_0, P_L, and P_R are the pressure of supply, atmosphere, left chamber, and right chamber, respectively.

B. MODELING OF THE CHAMBERS

The cylinder model can be divided into two parts: chambers and piston. By utilizing energy-conservation and energy-continuity laws, the pressure dynamics of the chambers can be built [32]. Considering the pressure P, volume V, mass m, and temperature T in Fig. 1, the ideal gas law can be described as:

$$P_i V_i = m_i R T_i \tag{3}$$

where $i = L$ or R denotes indices of two chambers. As the air flow process is assumed as adiabatic and the temperature change in each chamber is negligible regarding the temperature of the air supply, the time derivative of the pressure can be described by deriving and incorporating (3) in energy laws and heat-transfer laws [32]:

$$\dot{P}_i = \gamma \frac{RT}{V_i} \dot{m}_i - \gamma \frac{P_i}{V_i} \dot{V}_i \tag{4}$$

If the initial position of the piston is in the middle of the cylinder, the volume of the chambers can be given by:

$$\begin{cases} V_L = A_L(\frac{L}{2} + z) \\ V_R = A_R(\frac{L}{2} - z) \end{cases} \tag{5}$$

where A_L and A_R are the effective cross-sectional areas of the piston, L is the piston length, and z is the piston position. The positive direction of the piston position is marked in Fig. 1. We can get $A_L = A_R = A$ as the effective cross-sectional areas of both chambers are completely same in a double rod-end cylinder. The time derivative of the pressures can be

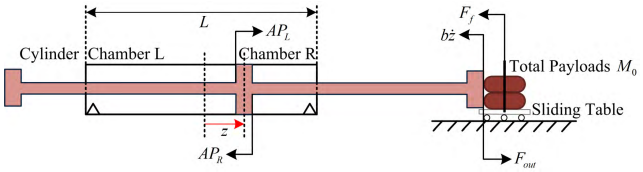

FIGURE 2. Force analysis of the piston.

expressed by incorporating (5) into (4):

$$\begin{cases} \dot{P}_L = \dfrac{\gamma RT}{A\left(\frac{L}{2} + z\right)} \left(\dot{m}_L - \dfrac{AP_L}{RT}\dot{z}\right) \\ \dot{P}_R = \dfrac{\gamma RT}{A\left(\frac{L}{2} - z\right)} \left(\dot{m}_R + \dfrac{AP_R}{RT}\dot{z}\right) \end{cases} \tag{6}$$

C. MODELING OF THE PISTON

As shown in Fig. 2, the piston movement can be described by using Newton's second law:

$$AP_L - AP_R - b\dot{z} - F_f + F_{out} = M_o \ddot{z} \tag{7}$$

where b represents the damping coefficient, F_f is the stiction force, F_{out} is the force generated by the atmosphere applied to the piston, and M_o is the total payloads including the piston and additional payloads. The stiction force F_f is ignored in the research as an anti-stiction cylinder is utilized in the experiment. By inserting the time derivative of (7) into (6), the piston model is given by:

$$\dddot{z} = \Psi + \frac{\gamma RT}{M_0}\left(\frac{\dot{m}_L}{\frac{L}{2} + z} - \frac{\dot{m}_R}{\frac{L}{2} - z}\right) \tag{8}$$

$$\Psi = -\frac{b}{M_0}\ddot{z} - \frac{\gamma A}{M_0}\left(\frac{P_L}{\frac{L}{2} + z} + \frac{P_R}{\frac{L}{2} - z}\right)\dot{z} \tag{9}$$

D. INTEGRATED MODEL

The integrated simulation frame is expressed in Fig. 3. MATLAB/Simulink is used to build the integrated model. In Fig. 3, the integrated model is divided into five parts: control signals, valve model, mass flow rate, cylinder model, and output signal. Each block in the simulation frame represents an m-file and they are linked by S-function package

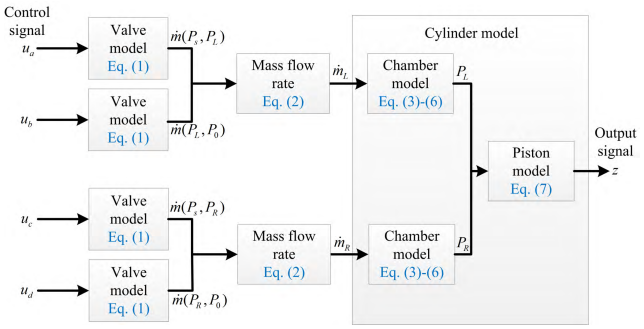

FIGURE 3. The integrated simulation frame.

TABLE 1. System parameters.

Symbol	System Parameters	Nominal Value
R	ideal gas constant	0.287 kJ/kg/K
γ	specific heat ratio	1.2
C_d	valve discharge coefficient	0.17×10^{-3}
T	stagnation temperature	293.15 K
S	orifice effective cross-sectional area	11×10^{-6} m^2
P_{cr}	critical pressure ratio	0.528
P_s	pressure of supply	3×10^5 Pa
P_0	pressure of atmosphere	1×10^5 Pa
A	piston effective cross-sectional area	8.5×10^{-5} m^2
L	piston length	0.1 m
b	damping coefficient	45 (N·s)/m

in the Simulink. Ode-45 (Dormand-Prince) and variable-step (0.1 ms to 0.2 ms) are chosen for the simulation. All the simulation parameters are listed in Table 1.

III. CONTROLLER DESIGN FOR THE POSITION TRACKING SYSTEM

In the past researches, three most-mentioned types of control strategies in the position tracking system are PID, fuzzy logic, and sliding mode. Traditional PID controller cannot achieve excellent control performance in the pneumatic systems as its strong nonlinearities. Salim *et al.* [23] propose an MN-PID controller which consists of a nonlinear-PID controller and a fuzzy logic controller in a pneumatic positioning system with a 5/3 bidirectional proportional valve and a double rod-end cylinder. However, the MN-PID method is hard to be utilized in an on-off valve controlled system as the highly nonlinear characteristic of the on-off valve. In the research of Hodgson *et al.* [15], a reasonable seven-mode sliding controller is proposed to control four on-off valves instead of the high-expense proportional valve in the pneumatic position tracking system. This method proposes a suitable way to arrange seven switching states in the whole control process and the experimental results are acceptable. According to

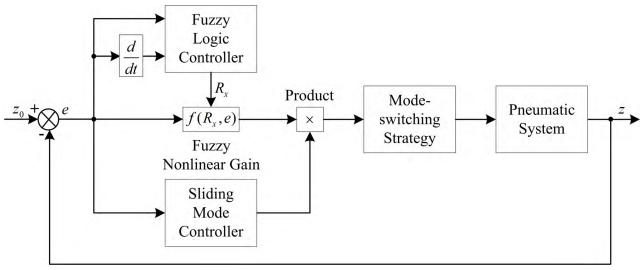

FIGURE 4. Block diagram of the mode-switching sliding controller with fuzzy nonlinear gain.

Hodgson *et al.*, about 1.9% positive overshoot is mentioned in the step response and more than 5% negative overshoot is observed. Although these results are far better than the results of the original three-mode method, the average 2% overshoot still needs improvement. In this paper, an improved mode-switching sliding controller with fuzzy nonlinear gain is put forward as shown in Fig. 4. Two controllers are used in the hybrid control scheme to reduce the overshoot and increase the response speed: a fuzzy logic controller which is used to generate the fuzzy nonlinear gain and a sliding mode controller which is used as the main controller for the four on-off valves. The fuzzy nonlinear gain has two major impacts: Firstly, the response speed can be increased by using the nonlinear gain. Secondly, the overshoot caused by the system uncertainty and strong nonlinear of the pneumatic system can be reduced as much as possible. The overshoots in the variable-payload experiment can be reduced without changing the control parameters. Additionally, the sliding mode controller is designed on the basis of seven-mode sliding controller from S. Hodgson *et al.* and several improvements are made to improve the control performance. In the end, the simulation results are charted to show the performance.

A. FUZZY NONLINEAR GAIN

The fuzzy nonlinear gain proposed in this paper is an adjustment to the sliding mode controller. The fuzzy tuning component consists of a fuzzy logic controller and a fuzzy nonlinear function. Three essential elements are taken into account while designing the component: error e (the difference between the reference position and the actual position), error rate $\dot{e}$ (time derivative of error), and variation of the total payloads M_0. The position error is expressed as:

$$e = z_0 - z \tag{10}$$

where z_0 is the position reference and z is the measured position. The fuzzy nonlinear function is written as:

$$f(R_x, e) = (R_x \cdot e)^2 + 1 \tag{11}$$

where R_x is the output of the fuzzy logic controller. The fuzzy nonlinear function is designed for two control results: fast response and minimum overshoot. When the error is big, the fuzzy nonlinear function will generate a significant nonlinear gain to increase the response speed. Then the error will

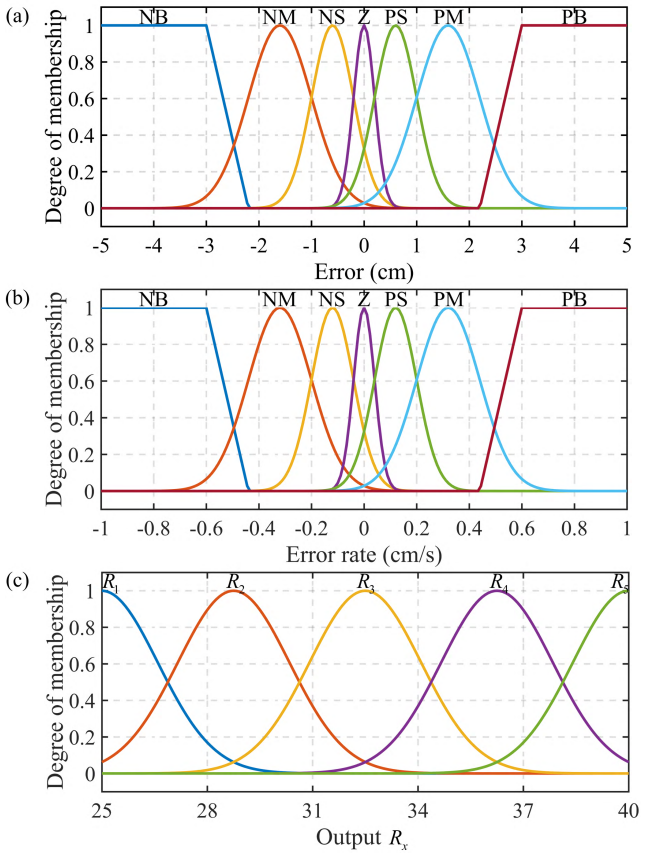

FIGURE 5. Fuzzy logic controller membership functions. (a) Input variable error, (b) Input variable error rate, (c) Output variable.

TABLE 2. Linguistic variables for error and error rate

Variable	Definition
NB	negative big
NM	negative medium
NS	negative small
Z	zero
PS	positive small
PM	positive medium
PB	positive big

TABLE 3. Fuzzy rules.

Error	ERROR RATE						
	NB	NM	NS	Z	PS	PM	PB
NB	R_4	R_4	R_4	R_5	R_4	R_4	R_4
NM	R_2	R_3	R_3	R_4	R_3	R_3	R_2
NS	R_1	R_2	R_2	R_2	R_2	R_2	R_1
Z	R_1	R_1	R_1	R_1	R_1	R_1	R_1
PS	R_1	R_2	R_2	R_2	R_2	R_2	R_1
PM	R_2	R_3	R_3	R_4	R_3	R_3	R_2
PB	R_4	R_4	R_4	R_5	R_4	R_4	R_4

decrease to a small amount, the output value of the function also declines with respect to the error. At the beginning of each movement, the higher nonlinear gain will raise the total opening time of the on-off valve and the piston will move much more rapidly. It is a corrective action for the primary controller. After the initial control stage, the gradually declining nonlinear gain will generate a smooth transition for the movement of the piston. This gain has the effect of making the piston move to the given position more rapidly. The smoother transition process also helps reduce the overshoot and avoid the oscillations.

In the fuzzy nonlinear function, another important part is the output of the fuzzy logic controller R_x. In this research, the designed controller is Mamdani-type [16]. The input and output of the Mamdani-type system are all linguistic variables. A defuzzification method is needed to get the digital output. The membership functions for the error, error rate, and the output R_x are demonstrated in Fig. 5. The linguistic variables for e and $\dot{e}$ are listed in Table 2.

As shown in Fig. 5, Gaussian and trapezoidal-shaped functions are selected for the input variables e and $\dot{e}$. The shape of the membership function has a significant influence on the performance of the fuzzy logic controller. The narrowest shape of Gaussian function appears near the zero point in Fig. 5 (a) and (b). This indicates that the control action is most sensitive when the error or error rate is approaching zero. When the error or error rate leaves zero point, the shapes of Gaussian functions become wider. In this stage, the control action becomes a little peaceful. The trapezoidal-shaped functions are designed to maintain the output. This design helps the system avoid generating great jitter during the starting stage and steady stage. Whereas, only Gaussian functions are used in the output variable R_x which is shown in Fig. 5 (c). The value of error, error rate, and R_x are decided by the experiments. The value of error ranges from -5 cm to 5 cm and the value of error rate ranges from -1 cm/s to 1 cm/s. The value of R_x ranges from 25 to 40 continuously. The fuzzy rules are summarized in Table 3. Several specific rules are designed based on the real practice to guarantee that the controller design can be used in the real experiment. When the error is zero (Z), the output is always R_1 which is the lowest value of output variable R_x. The smallest value of R_x will make the piston reach the reference position steadily and the overshoot is avoided. When the error is big (NB or PB) and the error rate is not zero (Z), the piston will move at a certain velocity by using the second largest value of R_x. The biggest value of R_x is designed in the condition that error is big (NB or PB) and error rate is zero (Z). The piston is just starting to move, and the biggest value of R_x helps increase the response speed. The defuzzification method is center of

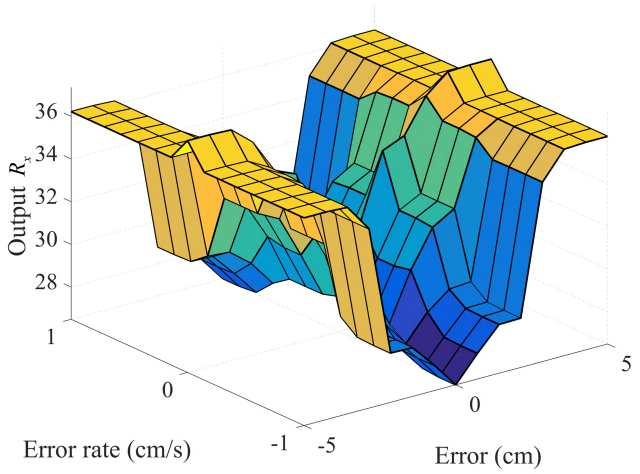

FIGURE 6. Control surface of the fuzzy logic controller.

gravity and the final control surface is shown in Fig. 6. This defuzzification method is simple and easy to be calculated.

After introducing the fuzzy logic output, we can find several features in the fuzzy nonlinear function which is shown in Fig. 7. When the error is zero, the function output is 1 which means no tuning for the following controller. Under a certain value of error, the function output varies with respect to the changing value of R_x. This characteristic gives the following controller a suitable corrective action.

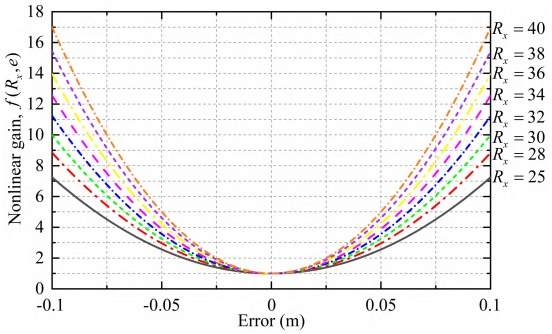

FIGURE 7. Characteristic of the fuzzy nonlinear function.

B. MODE-SWITCHING STRATEGY DESIGN

As mentioned in Fig. 1, four discrete control signals are set to control the valves. There are totally nine switching modes of the four on-off valves from the study of Le *et al.* [33]. According to Hodgson *et al.* [15], only seven switching modes are considered effective for the valves. These modes have different effects on the actuator and they are summarized in Table 4. For mode M_1, the left chamber is pressurized and the right chamber is exhausted at the same time. In this mode, the piston will move rapidly rightwards. Whereas, the left chamber is pressurized and the right chamber is closed in mode M_2. The control effect of mode M_2 is weaker than mode M_1. The piston will move slightly rightwards in this mode. For mode M_3, the right chamber is exhausted

TABLE 4. 7 switching modes of four valves.

	M_1	M_2	M_3	M_4	M_5	M_6	M_7
u_a	1	1	0	0	0	0	0
u_b	0	0	0	0	0	1	1
u_c	0	0	0	0	1	0	1
u_d	1	0	1	0	0	0	0

and the left chamber is closed. The control effect of mode M_3 is similar to mode M_2. The piston will move slightly rightwards in this mode too. In mode M_4, both chambers are closed, and the piston will not move. For mode M_7, the left chamber is exhausted and the right chamber is pressurized at the same time. In this mode, the piston will move rapidly leftwards. Whereas, the right chamber is pressurized and the left chamber is closed in mode M_5. The control effect of mode M_5 is weaker than mode M_7. The piston will move slightly leftwards in this mode. For mode M_6, the left chamber is exhausted and the right chamber is closed. The control effect of mode M_6 is similar to mode M_5. The piston will move slightly leftwards in this mode too.

In traditional PWM control, PWM 'period' T_t represents one control period for the actuator. As shown in Fig. 8 (a), the duty cycle D of the original mode-switching method from Hodgson *et al.* [15] is always 100%. In this paper, the duty cycle should be changeable to suit the fuzzy tuning method. So we improve the original mode-switching method in Fig. 8 (a) with changeable duty cycle. Fig. 8 (b) shows the detailed mode-switching method with changeable duty cycle D. This mode is denoted as mode M_1^D. Other corresponding modes are denoted with the superscript D too.

Fig. 9 shows the new mode-switching strategy for four on-off valves. Two dimensions are designed in the strategy for properly arranging the modes. One dimension is the sliding function s. The sliding function s for the new mode-switching strategy is designed as:

$$s = \frac{\ddot{e}}{\zeta^2} + \frac{2\rho\dot{e}}{\zeta} + e \tag{12}$$

where $\dot{e} = \dot{z}_0 - \dot{z}$, $\ddot{e} = \ddot{z}_0 - \ddot{z}$, and ζ ($\zeta > 0$) and ρ($\rho > 0$) are the sliding function parameters. The regimes of the sliding function s represent the corresponding control effect for the piston. When $|s| > \alpha$ (α is the mode-switching strategy parameter), M_7^D and M_1^D are arranged in the corresponding regimes as shown in Fig. 9. In these regimes, $|s|$ is quite large and fast movement of the piston is required. For mode M_7^D, the piston will move rapidly leftwards. For mode M_1^D, the piston will move rapidly rightwards. When $|s|$ is extremely small, the position response is approximately reaching the steady state. So when $|s| < \chi$ (χ is the mode-switching strategy parameter), M_4^D is arranged to close all the

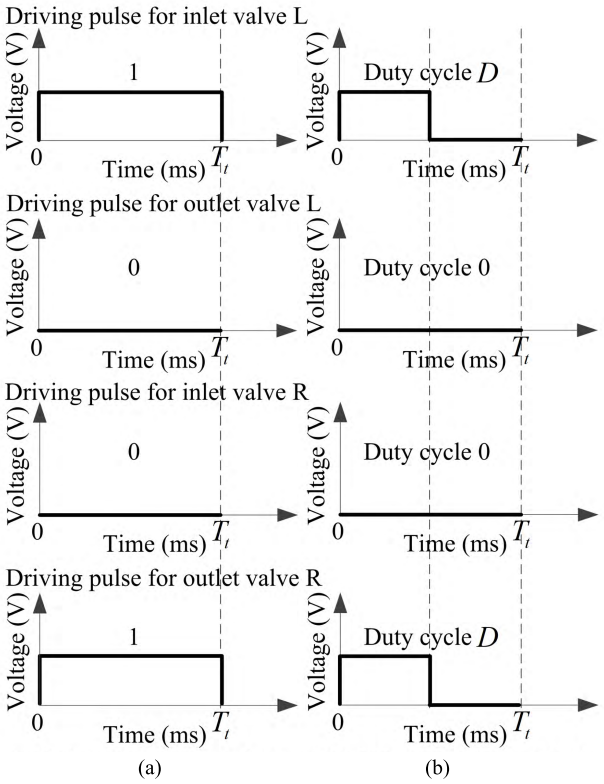

FIGURE 8. Comparison of the original mode-switching method (Mode M_1) and mode-switching method with duty cycle D (Mode M_1^D). (a) Original mode-switching method (Mode M_1). (b) Mode-switching method with duty cycle D (Mode M_1^D).

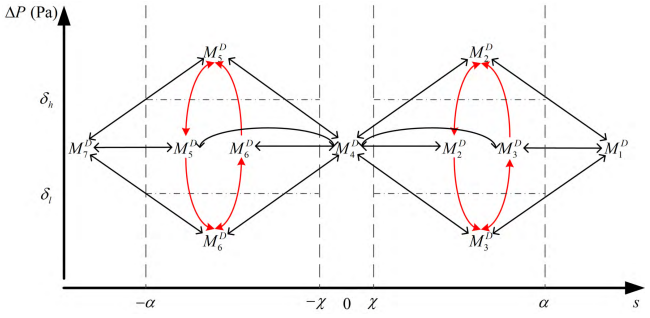

FIGURE 9. Mode-switching strategy for four on-off valves.

valves. Both chambers are closed in this mode, and the piston will stop moving. For the three regimes mentioned above, another dimension ΔP is not used. Pressure difference ΔP for the chambers is defined as [15]:

$$\begin{aligned}\Delta P &= (P_S - P_L) - (P_R - P_0) = (P_S + P_0) - (P_L + P_R) \\ &= P_{ou} - P_{ch} \end{aligned} \tag{13}$$

where P_{ou} is the sum of supply and atmosphere pressure, P_{ch} is the sum of the pressures of both chambers. ΔP represents the pressure difference between P_{ou} and P_{in}. Pressure difference ΔP is only valid in $-\alpha \le s \le -\chi$ and $\chi \le s \le \alpha$. Two pressure parameters are introduced to categorize the modes: δ_h and $\delta_l(\delta_h > \delta_l)$. In the regime of $-\alpha \le s \le -\chi$ and $\Delta P > \delta_h$, the piston needs to move slightly leftwards and the pressure difference needs to be decreased. So mode M_5^D is set in this regime. For mode M_5^D, right chamber is pressurized and left chamber is closed. The piston will move slightly leftwards. In this mode, the pressure of right chamber is increased and the pressure of left chamber is unchanged. According to (13), pressure difference is decreased. When the pressure difference is decreased to $\delta_l \le \Delta P \le \delta_h$, mode M_5^D is kept using to avoid the oscillation caused by frequently mode switch. Similarly, in the regime of $-\alpha \le s \le -\chi$ and $\Delta P < \delta_l$, the piston need to move slightly leftwards and the pressure difference need to be increased. Mode M_6^D is arranged in this regime. For this mode, left chamber is exhausted and right chamber is closed. The piston will move slightly leftwards in this mode too. In this mode, the pressure of left chamber is decreased and the pressure of right chamber is unchanged. Pressure difference is increased based on (13). Mode M_6^D is also maintained in $\delta_l \le \Delta P \le \delta_h$ for less oscillations. This hysteresis control method is summarized as:

$$H = \begin{cases} M_5^D, & \Delta P > \delta_h \\ M_6^D, & \Delta P < \delta_l \\ \text{No change}, & \delta_l \le \Delta P \le \delta_h \end{cases} \tag{14}$$

The hysteresis control method helps the system reduce the switching times of the valves greatly when the actual position of the piston is reaching the reference. As a result, the stability of the control process is much improved. The regime of $\chi \le s \le \alpha$ is similar to $-\alpha \le s \le -\chi$ as shown in Fig. 9. Mode M_2^D is set in $\Delta P > \delta_h$ and $\delta_l \le \Delta P \le \delta_h$. Mode M_3^D is set in $\Delta P < \delta_l$ and $\delta_l \le \Delta P \le \delta_h$. The hysteresis control method is also applied in these regimes. In Fig. 9, the regimes are divided by the dashed lines. The possible control paths including the hysteresis control method are marked out.

C. SLIDING MODE CONTROLLER DESIGN

The sliding mode function for the new mode-switching strategy is proposed in (12). An exponential approach law [3] for sliding mode controller is used to guarantee the dynamic quality of the sliding process and reduce the high-frequency jitter. The exponential approach law is written as:

$$\dot{s} = -\varphi \,\mathrm{sgn}(s) - \omega s \tag{15}$$

where $\varphi(\varphi > 0)$ and $\omega(\omega > 0)$ are exponential approach law parameters. z can be obtained by substituting the time derivative of (12) into (15):

$$\dddot{z} = \dddot{z}_0 + 2\rho\zeta\ddot{e} + \zeta^2\dot{e} + \varphi\zeta^2\mathrm{sgn}(s) + \omega\zeta^2 s = Y(z) \tag{16}$$

The system dynamics can be obtained by substituting (2) into (8):

$$\dddot{z} = \begin{cases} \Psi + g_i, & \text{mode } M_i^D (i = 1, 2 \text{ and } 3) \\ \Psi, & \text{mode } M_4^D \\ \Psi - g_i, & \text{mode } M_i^D (i = 5, 6 \text{ and } 7) \end{cases} \tag{17}$$

where

$$g_1 = \frac{\gamma RT}{M_0}\left(\frac{\dot{m}(P_s, P_L)}{\frac{L}{2}+z} + \frac{\dot{m}(P_R, P_0)}{\frac{L}{2}-z}\right),$$
$$g_2 = \frac{\gamma RT}{M_0}\frac{\dot{m}(P_s, P_L)}{\frac{L}{2}+z}, \quad g_3 = \frac{\gamma RT}{M_0}\frac{\dot{m}(P_R, P_0)}{\frac{L}{2}-z},$$
$$g_5 = \frac{\gamma RT}{M_0}\frac{\dot{m}(P_s, P_R)}{\frac{L}{2}-z}, \quad g_6 = \frac{\gamma RT}{M_0}\frac{\dot{m}(P_L, P_0)}{\frac{L}{2}+z},$$

and

$$g_7 = \frac{\gamma RT}{M_0}\left(\frac{\dot{m}(P_L, P_0)}{\frac{L}{2}+z} + \frac{\dot{m}(P_s, P_R)}{\frac{L}{2}-z}\right).$$

As $-\frac{L}{2} \le z \le \frac{L}{2}$, $\frac{L}{2}+z$, and $L/2-z$ are non-negative. All the mass flow rates are non-negative as $P_0 \le P_L \le P_s$ and $P_0 \le P_R \le P_s$. So all the g_i functions are non-negative. The sliding mode control law u is deduced by simplifying the system into three basic switching modes: mode M_1^D, M_4^D, and M_7^D. The model can be described as [34]:

$$\dddot{z} = \begin{cases} \Psi + g_1 u, & u \ge 0 \\ \Psi + g_7 u, & u < 0 \end{cases} \tag{18}$$

The sliding mode control law can be achieved by substituting (16) into (18):

$$u_{eq}^{+/-} = \frac{Y(z) - \Psi}{g^{+/-}} \tag{19}$$

where $g^{+/-} = \begin{cases} g_1, u \ge 0 \\ g_7, u < 0. \end{cases}$ Equation (19) represents that the sign of sliding mode control law u is changing according to the actual condition of the control system. When the sign of the sliding function s is non-negative, the piston is moving rightwards and u is also non-negative. When the sign of the sliding function s is negative, the piston is moving leftwards and u is also negative. Before utilizing the fuzzy nonlinear gain, a conversion formula is proposed to get the duty cycle D_0:

$$D_0 = \begin{cases} \frac{g_1}{g_i}u, & s \ge 0 \\ -\frac{g_7}{g_i}u, & s < 0 \end{cases} \tag{20}$$

where $i \in \{1, 2, 3, 5, 6, 7\}$. Then the actual duty cycle D for the mode-switching strategy with the fuzzy nonlinear gain can be given by:

$$D = D_0 \cdot f(R_x, e) \tag{21}$$

As all the g_i functions are non-negative, D_0 is non-negative. The fuzzy nonlinear gain $f(R_x, e)$ is non-negative and the duty cycle D is non-negative. A limiter is utilized to make sure that $D \le 1$:

$$D = \begin{cases} 1, & D \ge 1 \\ D, & 0 \le D < 1 \end{cases} \tag{22}$$

The Lyapunov-like function is used to verify the stability:

$$V = \frac{1}{2}s^2 \tag{23}$$

and

$$\dot{V} = s\dot{s} \tag{24}$$

Considering the sliding function (12) and (15), we can get

$$\dot{V} \le -\varphi|s| - \omega s^2 = -\frac{\omega}{2}V - \varphi|s| \le -\frac{\omega}{2}V \tag{25}$$

On the basis of lemma [35], for $V : [0, \infty) \in R$, the solution of $\dot{V} \le -\theta V + f, \forall t \ge t_0 \ge 0$ is

$$V(t) \le e^{-\theta(t-t_0)}V(t_0) + \int_{t_0}^{t} e^{-\theta(t-\tau)}f(\tau)d\tau \tag{26}$$

Proof of the Lemma: assume that $\phi(t)\dot{V} + \theta V - f$, then $\phi(t) \le 0$. The solution of $\dot{V} = -\theta V + f + \phi$ is:

$$V(t) = e^{-\theta(t-t_0)}V(t_0) + \int_{t_0}^{t} e^{-\theta(t-\tau)}f(\tau)d\tau + \int_{t_0}^{t} e^{-\theta(t-\tau)}\phi(\tau)d\tau \tag{27}$$

As $\phi(t) < 0$ and $\forall t \ge t_0 \ge 0$, then

$$V(t) \le e^{-\theta(t-t_0)}V(t_0) + \int_{t_0}^{t} e^{-\theta(t-\tau)}f(\tau)d\tau \tag{28}$$

If $f = 0$, the solution of $\dot{V} \le -\theta V$ is

$$V(t) \le e^{-\theta(t-t_0)}V(t_0) \tag{29}$$

If θ is positive, $V(t)$ will converge to 0 in exponential form. If the parameters are $\theta = \omega/2, f = 0$, then (25) can be obtained by:

$$V(t) \le e^{-\frac{\omega}{2}(t-t_0)}V(t_0) \tag{30}$$

V(t) will converges to 0 in the form of exponent. The sliding surface $s = 0$ is able to be reached in a limited time with the exponential approach law. Parameter φ determines the convergence velocity if the system is close to $s = 0$. Parameter ω determines the convergence velocity on the condition that $|s|$ is large.

D. PARAMETERS SELECTION

In this section, several suitable methods for parameters selection are discussed. Firstly, for the mode-switching strategy, mode-switching strategy parameters α and χ are decided on the basis of position errors. Parameter χ is selected according to the minimal absolute error e_{ma}. When the system is in the regime of $|s| < \chi$, the position response is approximately reaching the steady state. In this state, the influence of e is actually bigger than $\dot{e}$ and $\ddot{e}$. In this research, $e_{ma} = 0.001$ m is selected for the simulations and experiments. So $\chi = e_{ma} = 0.001$ is used to guarantee the accuracy of the system. Parameter α is the threshold between rapid control action and slight control action. Too large α or too small α may all lead to instability. As s is related

to the sliding function parameters ζ and ρ, Parameter α is decided after choosing ζ and ρ. Secondly, pressure parameters δ_h and δ_l are chosen based on the balanced pressure P_b. P_b can be measured by pressuring and exhausting a chamber with fixed volume at the same time. The pressure variation is approximately linear around this pressure. Assume that both chamber pressures of the cylinder are P_b, the balanced pressure δ_b for ΔP is obtained by:

$$\delta_b = P_s + P_0 - 2P_b \tag{31}$$

Then the equations for δ_h and δ_l are given by:

$$\begin{cases} \delta_h = \delta_b + \dfrac{P_s - P_0}{4} \\ \delta_l = \delta_b - \dfrac{P_s - P_0}{4} \end{cases} \tag{32}$$

The system pressures are $P_s = 3 \times 10^5$ Pa, $P_0 = 1 \times 10^5$ Pa, and $P_b = 2.431 \times 10^5$ Pa in the research. $\delta_b = -0.86 \times 10^5$ Pa, $\delta_h = -0.36 \times 10^5$ Pa, and $\delta_l = -1.36 \times 10^5$ Pa are selected for the following simulations and experiments. Thirdly, the procedure of selecting sliding function parameters (ζ and ρ) and exponential approach law parameters (φ and ω) is shown in Fig. 10. Detailed values will be discussed in the following sections. Additionally, the PWM period T_t is selected based on the opening and closing time of the on-off valve. A fast on-off valve with 1 ms opening time and 1ms closing time is used in the experimental setup, so $T_t = 10$ ms is chosen.

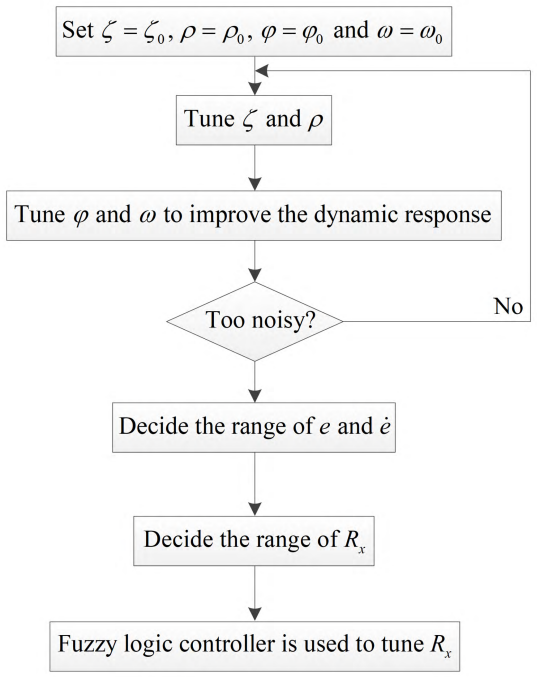

FIGURE 10. Procedure of parameters selection.

E. SIMULATION RESULTS

Two simulations are designed to show the characteristics of the proposed mode-switching sliding control with fuzzy nonlinear gain. In the first simulation, the proposed scheme, original seven-mode sliding controller from Hodgson *et al.* [15] and conventional PID controller are utilized to track a step pulse reference. Seven-mode sliding controller uses the same mode-switching method from Hodgson *et al.* which is mentioned in Table 4. The PID control law used in the research is written as:

$$u(t) = K_P e(t) + K_I \int_0^t e(t)dt + K_D \dot{e}(t) \tag{33}$$

where $u(t)$ is the control signal, $e(t)$ is the position error, and K_P, K_I, and K_D are PID controller parameters. In the PID controller, mode M_1, M_7, and M_4 are used to control the valves. The total payloads M_o for the simulations are 1.25 kg including piston weights of 0.25 kg and additional weights of 1 kg. In the first simulation, the control parameters are selected as $\alpha = 0.08$, $\chi = 0.001$, $\delta_b = -0.86 \times 10^5$ Pa, $\delta_h = -0.36 \times 10^5$, $\delta_l = -1.36 \times 10^5$, $\zeta = 110$, $\rho = 0.5$, $\varphi = 0.1$, $\omega = 3$, and $T_t = 10$. The simulation results are shown in Fig. 11. For the proposed scheme, there is almost no overshoot and oscillation. In the rising period, the piston reaches the reference position in 0.22 s. For the original seven-mode sliding controller, the overshoot problem is also hard to be observed in the simulation. The rising time for seven-mode method is about 0.25 s. The position response controlled by PID controller shows a large overshoot and oscillation phenomenon. The piston takes about 0.69 s to reach the steady state, and the biggest overshoot is about

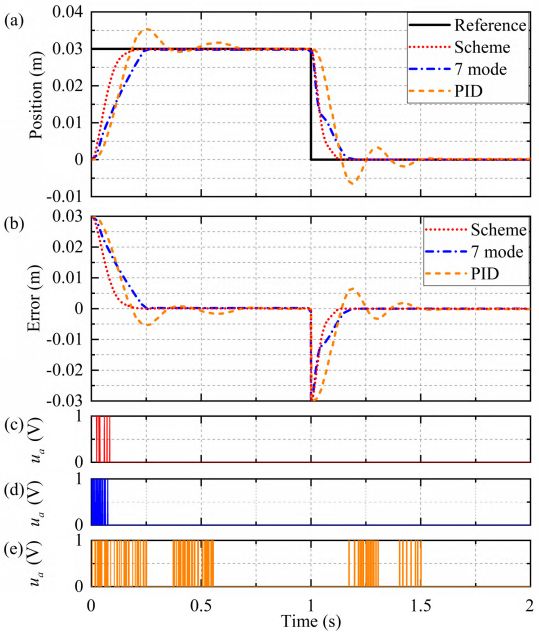

FIGURE 11. Simulation results of the step response for mode-switching sliding control with fuzzy nonlinear gain, original seven-mode sliding controller from Hodgson *et al.*, and conventional PID controller. (a) Position, (b) Position error, (c) Input voltage of inlet valve L for mode-switching sliding control with fuzzy nonlinear gain, (d) Input voltage of inlet valve L for original seven-mode sliding controller from Hodgson *et al.*, (e) Input voltage of inlet valve L for conventional PID controller.

0.005 m (16.67%). The PID parameters are selected as $K_P = 0.2, K_I = 0.02, K_D = 0.001$, and $T_t = 10$. This set of PID parameters is chosen by experience and more than one set of parameters are tested in the simulation. The presented parameters are the optimal set according to the control performance. The rising time is shorter and the response curve is smoother in the proposed scheme. The fuzzy nonlinear gain shortens the response time. The overshoot problem of the seven-mode method will be discussed in the experimental part. The overshoot problem of PID controller is caused by two reasons: firstly, only three basic modes are used in PID controller. When the error is approaching zero, the controller keeps using mode M_1 or M_7 to drive the valves. These modes will generate a great mass flow to the chambers, and the control action is too big for the system. Secondly, traditional PID controller is inappropriate for a greatly nonlinear system. Fig. 11 (c), (d), and (e) shows the switching of the inlet valve L for three methods. The proposed scheme and seven-mode method both lower the switching times of the valves.

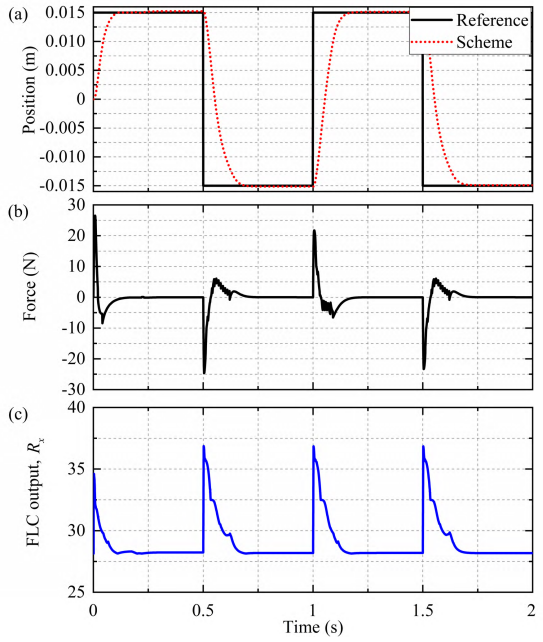

FIGURE 12. Simulation results of the step response. (a) Position, (b) Force, (c) FLC output.

Another simulation of tracking the step pulse reference is shown in Fig. 12. From Fig. 12 (c), the FLC output decreases from the biggest value to the minimum value with respect to the variation of the position response. The force which is produced to move the piston to the given position is shown in Fig. 12 (b). The rising time of this simulation is averaging 0.22 s with 0.03 m moving distance. This simulation uses the same parameters of the first simulation and the total payloads are 1.25 kg. Both simulations present the great performance of the proposed method.

Indeed, several assumptions mentioned in Section II cannot be guaranteed in the real experiment. To make the experiment more close to the assumptions, we apply the following measures: sealing glue is used to make sure the system is airtight; refrigerated air dryer is used to make sure the minimal temperature change inside the chambers; an anti-stiction actuator and lubricating oil are used to make sure the stiction force of the piston is negligible. The experimental system is more reliable with these measures.

IV. EXPERIMENTAL SETUP

Overall experimental setup is shown in Fig. 13. The pneumatic instruments consist of four 2/2 on-off solenoid valves (Matrix model MX 821.103C2XX) with speed-up driving control which has response time of less than 1ms in the opening and closing, a double-acting, double rod-end, and anti-stiction cylinder (Airpel model M24D100.0D) which has a length of 100mm and a rod diameter of 24mm, a sliding table with some standard weights, three silicon-diffused pressure sensors, a linear position sensor, an air compressor (DENAIR model DVA-11A), a compressed air tank, an air-drying machine, and a Filter-Regulator-Lubricator (FRL) unit. In the electrical setup, a real-time industrial controller (NI model cRIO-9074) which has a reconfigurable FPGA module is applied as the main controller. A bi-directional 5 V/TTL digital card (NI model NI-9401) and a 16-bit analog-input differential card (NI model NI-9205) are installed on the controller for sending and collecting signals. A sensor circuit, power circuit, and a valve driving circuit are also designed for the signal conditioning. The real control system is shown in Fig. 14. Programs are deployed on NI Labview 11. The detailed tasks for PC, cRIO-9074 RT, and FPGA are shown in Fig. 15. Logic control, time sequence control, and data calculation of the proposed scheme are carried out on FPGA. The procedures of Reading data from NI 9205 and writing data on NI 9401 are also executed on FPGA. The FPGA platform is known for its high reliability in sequential control. The precise time sequence control ensures the reliability of algorithm execution. This hardware platform can achieve both high real-time performance and fast response in electro-pneumatic systems.

V. EXPERIMENTAL RESULTS AND DISCUSSION

Five experiments are carried out on the experimental setup mentioned above in the section. Firstly, a contrast experiment is designed to show the advantage of the proposed scheme over other methods. The control performance is shown in Fig. 16 (a). In this experiment, the total payloads are 1.25 kg. The parameters are chosen as $\alpha = 0.08$, $\chi = 0.001$, $\delta_b = -0.86 \times 10^5$ Pa, $\delta_h = -0.36 \times 10^5$, $\delta_l = -1.36 \times 10^5$, $\zeta = 50$, $\rho = 1$, $\varphi = 1$, $\omega = 5$, and $T_t = 10$. Only 0.73% overshoot and 0.22 mm steady-state error are observed in the rising stage of the position controlled by the proposed scheme. The settling time is about 0.22 s. These results are all smallest of the three control methods. For the position response controlled by the original seven-mode

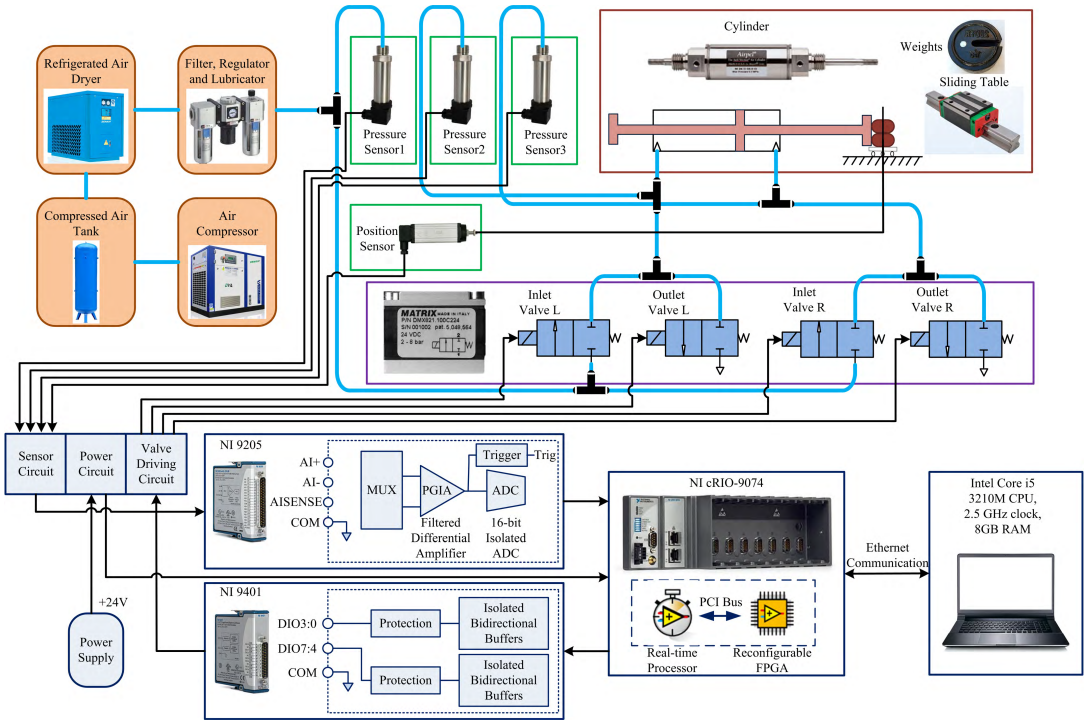

FIGURE 13. Overall experimental setup.

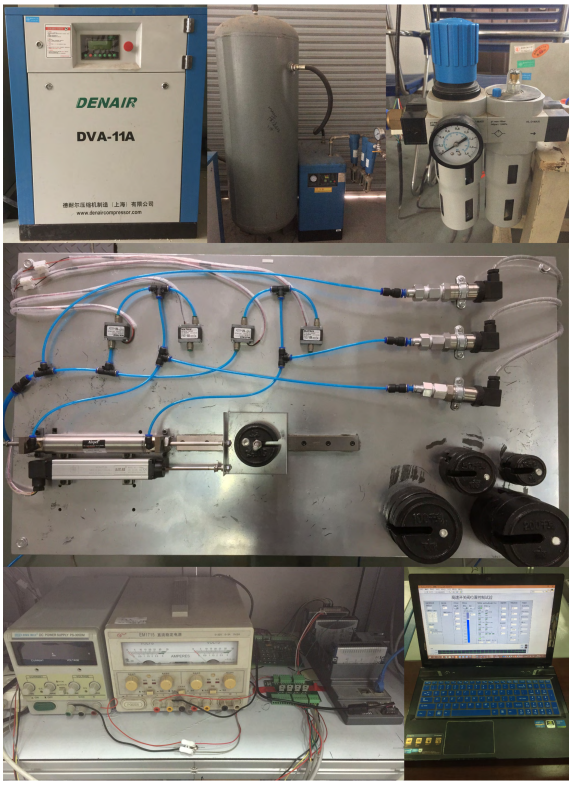

FIGURE 14. Pictures of the real system.

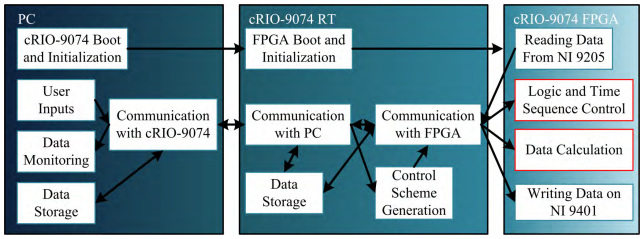

FIGURE 15. Assignments deployed on cRIO-9074 RT and FPGA.

sliding controller from Hodgson *et al.* [15], the overshoot is about 0.89 mm (2.97%) and the settling time is nearly 0.4 s in the rising stage. In the decreasing period, a bigger overshoot (4.53%) is observed in the position response controlled by the seven-mode method. Whereas, only 0.89% overshoot is found in the position response controlled the proposed scheme. Two aspects lead to improving control performance: fuzzy nonlinear gain and improved mode-switching strategy. After utilizing the fuzzy nonlinear gain, the response speed is clearly increased and the overshoot is reduced to the minimum. The new mode-switching strategy including the hysteresis control method also has a great effect on reducing the overshoot. For the PID controller with 3 basic switching modes (mode M_1, M_4, and M_7), parameters are chosen as $K_P = 0.1$, $K_I = 0.01$, and $K_D = 0.001$. As explained in the simulation part, the conventional PID controller cannot achieve good performance in the nonlinear system.

The second experiment is tracking the step pulse reference which is shown in Fig. 17. FLC output decreases from the biggest value (about 37.21) to the minimum value (about 27.72) with respect to the variation of the position response. The settling time of this experiment is averaging 0.21 s with 0.03 m moving distance. The averaging overshoot is about 0.8% and steady-state error is 0.5 mm.

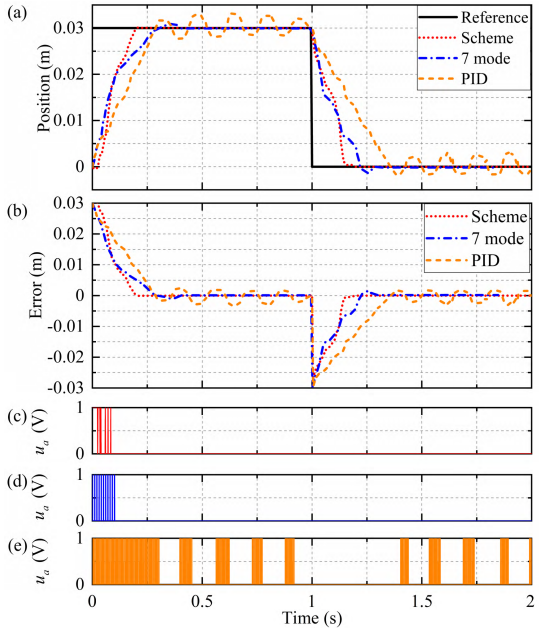

FIGURE 16. Experimental results of the step response for mode-switching sliding control with fuzzy nonlinear gain, original seven-mode sliding controller from Hodgson *et al.*, and conventional PID controller. (a) Position, (b) Position error, (c) Input voltage of inlet valve L for mode-switching sliding control with fuzzy nonlinear gain, (d) Input voltage of inlet valve L for original seven-mode sliding controller from Hodgson *et al.*, (e) Input voltage of inlet valve L for conventional PID controller.

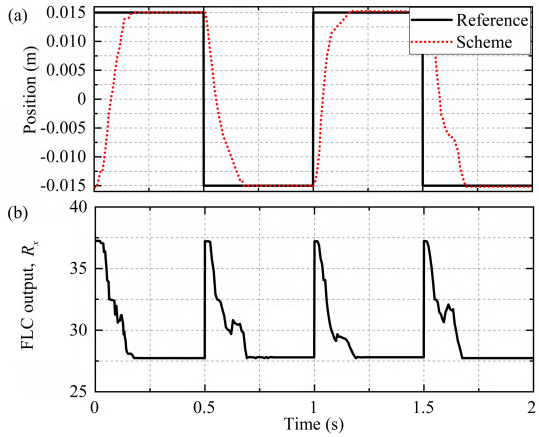

FIGURE 17. Experimental results of the step response. (a) Position, (b) FLC output.

In the third experiment of tracking a dynamic pulse reference, overshoots between 0.9% and 6.57% are observed. Steady-state errors are between 0.5 mm and 1.2 mm. The smallest settling time is 0.11 s and the biggest settling time is 0.71 s. The FLC output ranges from 36.23 to 27.79. The experimental results are presented in Fig. 18.

An experiment of sinusoidal tracking response is tested. The frequency of the sine wave is set to 0.33 Hz. As shown in Fig. 19, the position response can tightly track the reference from 0.03 m to -0.03 m. The position error is ranging from 4.13 mm to -3.57 mm. Parameters and total payloads for the

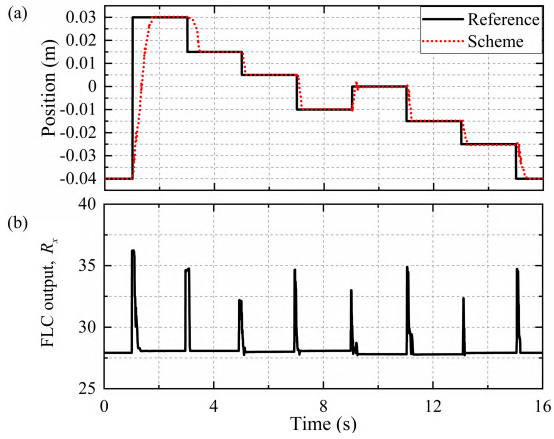

FIGURE 18. Experimental results of the dynamic step response. (a) Position, (b) FLC output.

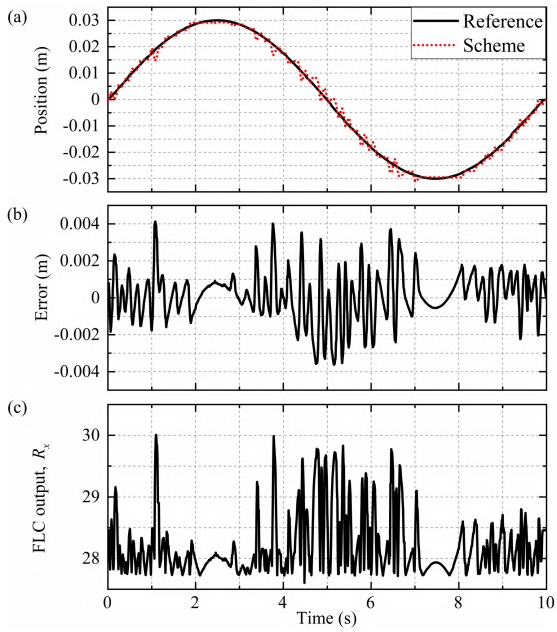

FIGURE 19. Experimental results of the sinusoidal response. (a) Position, (b) Position error, (c) FLC output.

second, third, and fourth experiment are the same as the first experiment.

In the last experiment, the tracking ability under different payloads is tested. Experimental results from the step pulse reference under different payloads are shown in Fig. 20. 1.25 kg, 3.25 kg, 6.25 kg, and 10.25 kg are the testing values of the total payloads. We keep using the same parameters of the first experiment. Only small overshoots and steady-state errors are observed in this experiment. In the rising period, the settling times are 0.22 s, 0.26 s, 0.3 s, and 0.325 s for the four payloads.

The experimental results indicate that the improved mode-switching sliding controller with the nonlinear gain generated by a fuzzy logic controller can track different kinds

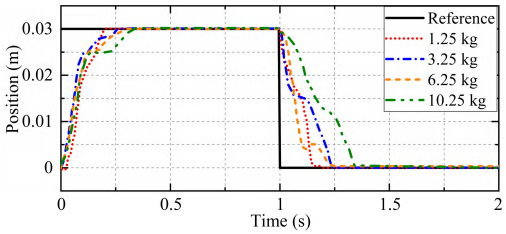

FIGURE 20. Experimental results of the step response under different payloads.

of reference under total payloads of 10.25 kg. The contrast experiment shows the improved performance of the new method. However, traditional PID controller cannot control the system since the high nonlinearity of the system. The proposed scheme also shows great performance when tracking dynamic pulse reference and sine wave reference. Maximum overshoot for tracking dynamic pulse reference is 6.57% and maximum position error for tracking sine wave reference is only 4.13 mm. The last experiment shows that the proposed scheme is able to handle different payloads.

We propose the novel method to solve the overshoot problem from the previous seven-mode method. There are totally two major contributions in the paper. Firstly, by utilizing the fuzzy nonlinear gain, the overshoot is reduced to the minimum in the step response and the settling time is also reduced. Only 0.89% positive overshoot is found in tracking the step response from 0.03 m to 0. While in the past research of seven-mode method from Hodgson *et al.*, about 1.9% positive overshoot is found in the same experiment. Moreover, the fuzzy nonlinear gain increases the opening time of the valves in the initial control period which leads to excellent control action and faster response. When the piston is approaching the given position, the fuzzy nonlinear gain reduces the valve action, and the overshoot is reduced. Secondly, the new mode-switching strategy for four on-off valves helps reduce the overshoot. The hysteresis controller is newly proposed in the mode-switching strategy and the key of reducing the oscillation of valves. Without the hysteresis controller, the system will be highly unstable and the valves will keep switching when the piston is reaching its given position. Compared to the original seven-mode method, the overshoots, steady-state errors, and settling time are all diminished. In addition, the logic control and accurate time sequence control are guaranteed by using FPGA platform. The improved mode-switching sliding control with fuzzy nonlinear gain is proven to be effective in terms of the simulation and experimental results.

VI. CONCLUSION

In this paper, a mode-switching sliding controller with fuzzy nonlinear gain is proposed to control a real-time electro-pneumatic position tracking system including four on-off valves and a double rod-end cylinder. The purpose of the new scheme is to enhance the tracking performance by reducing overshoots and increasing response speed in tracking different kinds of reference. The fuzzy nonlinear gain is generated by a fuzzy logic controller and a fuzzy nonlinear function. The major impacts of the fuzzy nonlinear

TABLE 5. Symbols.

Symbol	Nomenclature
$\dot{m}(P_{in}, P_{out})$	air mass flow rate passing through the valve orifice (kg/s)
P_{in}	input pressure of the valve (Pa)
P_{out}	output pressure of the valve (Pa)
C_d	discharge coefficient of the valve
S	effective cross-sectional area of the orifice (m^2)
T	stagnation temperature (K)
γ	specific heat ratio
R	ideal gas constant (kJ/kg/K)
P_c	specific pressure ratio
P_{cr}	Critical pressure ratio
m_L, m_R, and m	mass of the chamber (kg)
$\dot{m}_L$ and $\dot{m}_R$	mass flow rate of the chamber (kg/s)
u_a, u_b, u_c, and u_d	control inputs for four valves
P_s and P_0	pressure of supply and atmosphere (Pa)
P_L, P_R, and P	pressure of the chamber (Pa)
V_L, V_R, and V	volume of the chamber (m^3)
A_L, A_R, and A	effective cross-sectional areas of the piston (m^2)
L	piston length (m)
z	piston position (m)
b	damping coefficient ((N·s)/m)
F_f	stiction force (N)
M_i	mode M_i ($i \in \{1,2,3,4,5,6,7\}$)
M_i^D	mode M_i^D ($i \in \{1,2,3,4,5,6,7\}$) with duty cycle D
s	sliding function
ζ, ζ_0, ρ_0, and ρ	sliding function parameters
α and χ	mode-switching strategy parameters
ΔP	pressure difference (Pa)
P_{ou}	sum of supply and atmosphere pressure (Pa)
P_{ch}	sum of left and right chamber pressure (Pa)
δ_h and δ_l	pressure parameters (Pa)
φ, φ_0, ω, and ω_0	exponential approach law parameters
g_i	g_i ($i \in \{1,2,3,5,6,7\}$) functions of mass flow rates (kg/s)
u and $u_{eq}^{+/-}$	control input
V and $\dot{V}$	Lyapunov-like function
e_{ma}	minimal absolute error (m)
P_b and δ_b	balanced pressures (Pa)
K_P, K_I, and K_D	PID controller parameters

gain are demonstrated by simulations and experiments. In addition, the mode-switching strategy is newly designed and the hysteresis control method is introduced to improve the performance. At last, the improved mode-switching sliding controller is combined with the fuzzy nonlinear gain and the system stability is demonstrated.

Simulation and experimental results including a contrast test have shown the advantage of the proposed scheme over the previous methods. In comparison with the original seven-mode method from Hodgson *et al.*, the proposed scheme shows smaller overshoots, steady-state errors, and settling time in tracking step reference. Additionally, the experimental results carried out on FPGA platform also show that the proposed method is able to track sine wave reference, dynamic step reference, and step reference with payloads up to 10.25 kg.

APPENDIX

See Table 5.

REFERENCES

[1] G. Belforte, S. Mauro, and G. Mattiazzo, "A method for increasing the dynamic performance of pneumatic servosystems with digital valves," *Mechatronics*, vol. 14, no. 10, pp. 1105–1120, 2004.

[2] J. F. Carneiro and F. G. De Almeida, "On the influence of velocity and acceleration estimators on a servopneumatic system behaviour," *IEEE Access*, vol. 4, pp. 6541–6553, 2016.

[3] Z. Lin, T. Zhang, and Q. Xie, "Intelligent real-time pressure tracking system using a novel hybrid control scheme," *Trans. Inst. Meas. Control*, to be published, doi: 10.1177/0142331217730886.

[4] S. R. Goldstein and H. H. Richardson, "A differential pulse-length modulated pneumatic servo utilizing floating-flapper-disk switching valves," *J. Basic Eng.*, vol. 90, no. 2, pp. 143–151, 1968.

[5] S. Nie, X. Liu, F. Yin, H. Ji, and J. Zhang, "Development of a high-pressure pneumatic on/off valve with high transient performances direct-driven by voice coil motor," *Appl. Sci.*, vol. 8, no. 4, p. 611, 2018.

[6] M. Fathi and F. Najafi, "Improved tracking accuracy of a pneumatic actuator on entire piston stroke by a modified fuzzy-PWM controller," *J. Brazilian Soc. Mech. Sci. Eng.*, vol. 39, no. 3, pp. 879–893, 2017.

[7] T. Noritsugu, "Development of PWM mode electro-pneumatic servomechanism. I: Speed control of a pneumatic cylinder," *J. Fluid Control*, vol. 17, no. 1, pp. 65–80, 1986.

[8] T. Noritsugu, "Development of PWN mode electro-pneumatic servomechanism. II: Position control of a pneumatic cylinder," *J. Fluid Control*, vol. 17, no. 2, pp. 7–31, 1987.

[9] Y. Zhu and B. Jin, "Analysis and modeling of a proportional directional valve with nonlinear solenoid," *J. Brazilian Soc. Mech. Sci. Eng.*, vol. 38, no. 2, pp. 507–514, 2016.

[10] J. Zhang, C. Lv, X. Yue, Y. Li, and Y. Yuan, "Study on a linear relationship between limited pressure difference and coil current of on/off valve and its influential factors," *ISA Trans.*, vol. 53, no. 1, pp. 150–161, 2014.

[11] K. Ahn and B. Lee, "Intelligent switching control of pneumatic cylinders by learning vector quantization neural network," *J. Mech. Sci. Technol.*, vol. 19, no. 2, pp. 529–539, 2005.

[12] M. Q. Le, M. T. Pham, R. Moreau, and T. Redarce, "Comparison of a PWM and a hybrid force control for a pneumatic actuator using on/off solenoid valves," in *Proc. IEEE/ASME AIM*, Montreal, ON, Canada, Jul. 2010, pp. 1146–1151.

[13] M. Bangaru and S. Devaraj, "Energy efficiency analysis of interconnected pneumatic cylinders servo positioning system," in *Proc. ASME*, Houston, TX, USA, 2015, p. V04AT04A034.

[14] T. Nguyen, J. Leavitt, F. Jabbari, and J. E. Bobrow, "Accurate sliding-mode control of pneumatic systems using low-cost solenoid valves," *IEEE/ASME Trans. Mechatronics*, vol. 12, no. 2, pp. 216–219, Apr. 2007.

[15] S. Hodgson, M. Q. Le, M. Tavakoli, and M. T. Pham, "Improved tracking and switching performance of an electro-pneumatic positioning system," *Mechatronics*, vol. 22, no. 1, pp. 1–12, 2012.

[16] M.-C. Shih and M.-A. Ma, "Position control of a pneumatic cylinder using fuzzy PWM control method," *Mechatronics*, vol. 8, no. 3, pp. 241–253, 1998.

[17] M.-K. Chang, "An adaptive self-organizing fuzzy sliding mode controller for a 2-DOF rehabilitation robot actuated by pneumatic muscle actuators," *Control Eng. Pract.*, vol. 18, no. 1, pp. 13–22, 2010.

[18] S. Yu, T. K. Chau, T. Fernando, A. V. Savkin, and H. H.-C. Iu, "Novel quasi-decentralized SMC-based frequency and voltage stability enhancement strategies using valve position control and FACTS device," *IEEE Access*, vol. 5, pp. 946–955, 2017.

[19] B. Satpati, C. Koley, and S. Datta, "Sensor-less predictive drying control of pneumatic conveying batch dryers," *IEEE Access*, vol. 5, pp. 3547–3568, 2017.

[20] G. Niu and X. Huang, "Failure prognostics of locomotive electro-pneumatic brake based on bond graph modeling," *IEEE Access*, vol. 5, pp. 15030–15039, 2017.

[21] A. Talhan and S. Jeon, "Pneumatic actuation in haptic-enabled medical simulators: A review," *IEEE Access*, vol. 6, pp. 3184–3200, 2018.

[22] M. F. Rahmat, S. N. Salim, N. H. Sunar, A. M. Faudzi, Z. H. Ismail, and K. Huda, "Identification and non-linear control strategy for industrial pneumatic actuator," *Int. J. Phys. Sci.*, vol. 7, no. 17, pp. 2565–2579, 2012.

[23] S. N. S. Salim, M. F. Rahmat, A. A. M. Faudzi, and Z. H. Ismail, "Position control of pneumatic actuator using an enhancement of NPID controller based on the characteristic of rate variation nonlinear gain," *Int. J. Adv. Manuf. Technol.*, vol. 75, nos. 1–4, pp. 181–195, 2014.

[24] B. Najjari, S. Barakati, A. Mohammadi, M. J. Futohi, and M. Bostanian, "Position control of an electro-pneumatic system based on PWM technique and FLC," *ISA Trans.*, vol. 53, no. 2, pp. 647–657, 2014.

[25] S. Hodgson, M. Tavakoli, M. T. Pham, and A. Leleve, "Nonlinear discontinuous dynamics averaging and PWM-based sliding control of solenoid-valve pneumatic actuators," *IEEE/ASME Trans. Mechatronics*, vol. 20, no. 2, pp. 876–888, Apr. 2015.

[26] J.-M. Ramos-Arreguin *et al.*, "Fuzzy logic hardware implementation for pneumatic control of one DOF pneumatic robot," in *Proc. MICAI*, Berlin, Germany, 2010, pp. 500–511.

[27] M. P. S. dos Santos and J. A. F. Ferreira, "Novel intelligent real-time position tracking system using FPGA and fuzzy logic," *ISA Trans.*, vol. 53, no. 2, pp. 402–414, 2014.

[28] E. E. Topçu, I. Yüksel, and Z. Kamiş, "Development of electro-pneumatic fast switching valve and investigation of its characteristics," *Mechatronics*, vol. 16, no. 6, pp. 365–378, 2006.

[29] M. Taghizadeh, A. Ghaffari, and F. Najafi, "Modeling and identification of a solenoid valve for PWM control applications," *Comptes Rendus Mécanique*, vol. 337, no. 3, pp. 131–140, 2009.

[30] B. W. Andersen and R. C. Binder, "The analysis and design of pneumatic systems," *J. Appl. Mech.*, vol. 34, no. 4, p. 1055, 1967.

[31] D. McCloy and H. R. Martin, "Static characteristics of valves," in *Control of Fluid Power: Analysis and Design*, 2nd ed. New York, NY, USA: Halsted Press, 1980, pp. 159–180.

[32] E. Richer and Y. Hurmuzlu, "A high performance pneumatic force actuator system: Part I—Nonlinear mathematical model," *J. Dyn. Syst., Meas., Control*, vol. 122, no. 3, pp. 416–425, 2000.

[33] M. Q. Le, M. T. Pham, R. Moreau, and T. Redarce, "Transparency of a pneumatic teleoperation system using on/off solenoid valves," in *Proc. IEEE RO-MAN*, Viareggio, Italy, Sep. 2010, pp. 15–20.

[34] X. Shen, J. Zhang, E. J. Barth, and M. Goldfarb, "Nonlinear model-based control of pulse width modulated pneumatic servo systems," *J. Dyn. Syst., Meas., Control*, vol. 128, no. 3, pp. 663–669, 2005.

[35] P. Ioannou and J. Sun, *Robust Adaptive Control*. Upper Saddle River, NJ, USA: Prentice-Hall, 1996, pp. 98–120.

ZHONGLIN LIN was born in Fuzhou, Fujian, China, in 1989. He received the B.S. and M.S. degrees from the Nanjing University of Aeronautics and Astronautics, Nanjing, China, in 2012 and 2015, respectively. He is currently with the Jiangsu Province Key Laboratory of Aerospace Power System, Nanjing University of Aeronautics and Astronautics. His main research interests include the areas of pneumatic control systems, system modeling and simulation, and the hardware-in-the-loop test of aero-engine.

TIANHONG ZHANG was born in Yizheng, Jiangsu, China. He received the B.S., M.S., and Ph.D. degrees from the Nanjing University of Aeronautics and Astronautics (NUAA), Nanjing, China, in 1991, 1994, and 2001, respectively. In 1994, he joined the College of Energy and Power Engineering, NUAA, where he has been a Professor since 2007. He is currently with the Jiangsu Province Key Laboratory of Aerospace Power System, Nanjing University of Aeronautics and Astronautics. He has published or co-authored over 80 technical papers in journals and conferences. His main research interests are test and control of aero-engine, system modeling and simulation, and embedded systems.

QI XIE was born in Suzhou, Jiangsu, China, in 1994. He received the B.S. degree from the Nanjing University of Aeronautics and Astronautics, Nanjing, China, in 2012. He is currently with the Jiangsu Province Key Laboratory of Aerospace Power System, Nanjing University of Aeronautics and Astronautics. His main research interests lie in the areas of active combustion control, the test of UV sensor, and the test of high-speed ON–OFF valve.

QINGYAN WEI was born in Guilin, Guangxi, China, in 1978. She received the B.S., M.S., and Ph.D. degrees from the Nanjing University of Aeronautics and Astronautics (NUAA), Nanjing, China, in 2000, 2005, and 2016, respectively. In 2005, she joined the College of Energy and Power Engineering, NUAA, as a Teacher. She is currently with the Jiangsu Province Key Laboratory of Aerospace Power System, Nanjing University of Aeronautics and Astronautics. She has published eight technical papers in journals and conferences. Her main research interests are the test of aero-engine systems, and system modeling and simulation.